Quaternary Science Reviews 250 (2020) 106699

Contents lists available at ScienceDirect

Quaternary Science Reviews

journal homepage: www.elsevier.com/locate/quascirev

East Asian monsoon changes early in the last deglaciation and insights into the interpretation of oxygen isotope changes in the Chinese stalagmite record

Yijia Liang [a, b, c], Kan Zhao [a, b, c, *], R. Lawrence Edwards [a, d], Yongjin Wang [a, b, c], Qingfeng Shao [a, b, c], Zhenqiu Zhang [a, b, c], Bin Zhao [a, b, c], Quan Wang [e, f], Hai Cheng [g], Xinggong Kong [a, b, c]

[a] School of Geography, Nanjing Normal University, Nanjing, 210023, China
[b] Key Laboratory of Virtual Geographic Environment (Nanjing Normal University), Ministry of Education, Nanjing, 210023, China
[c] Jiangsu Center for Collaborative Innovation in Geographical Information Resource Development and Application, Nanjing, 210023, China
[d] Department of Earth and Environmental Sciences, University of Minnesota, Minneapolis, MN, 55455, USA
[e] Chongqing Key Laboratory of Earth Surface Processes and Environmental Remote Sensing in Three Gorges Reservoir Area, Chongqing, 401331, China
[f] School of Geography and Tourism, Chongqing Normal University, Chongqing, 401331, China
[g] Institute of Global Environmental Change, Xi'an Jiaotong University, Xi'an, 710054, China

ARTICLE INFO

Article history:
Received 25 April 2020
Received in revised form
31 October 2020
Accepted 1 November 2020
Available online 11 November 2020

Keywords:
Chinese stalagmite
East Asian summer monsoon
Oxygen isotope interpretation
Last deglaciation
Heinrich stadial 1

ABSTRACT

Stalagmite oxygen isotope ($\delta^{18}O$) records have enhanced our understanding of the history of the East Asian monsoon. However, abrupt changes in the monsoon are not constrained well enough to address certain issues and there are still unknowns in the interpretation of cave $\delta^{18}O$ records. Here we present a new high-resolution stalagmite record from Shima Cave, central China. Anchored with 24 $^{230}Th/U$ dates, our sample grew from 19.7 to 17.8 ka and from 16.3 to 13.3 ka, covering much of the early portion of the last deglaciation with a temporal resolution of 7 years. Using this record and other available Asian $\delta^{18}O$ records, we test model predictions for shifts in $\delta^{18}O$ in Asian caves and further investigate monsoon variations on centennial to decadal timescales during the early portion of the last termination. We conclude the following regarding the interpretation of $\delta^{18}O$ in Chinese caves. Two mechanisms affect $\delta^{18}O$: changes in the fraction of monsoon rainfall in annual totals (the Wang-Cheng mechanism) and changes in the amount of rainout between tropical sources and cave sites (the Yuan mechanism). The former is caused by changes in the seasonal migration of the sub-tropical jet and likely has a smaller effect on cave $\delta^{18}O$ than the latter. The latter involves changes in rainout from *both* the Pacific and the Indian Ocean sources. Precisely how that change in rainout is partitioned between sources and cave sites is not fully understood; however, it is clear that some of the change takes place in China; i.e. it is not restricted to upstream sites. Rough calculations for our site suggest that mean annual rainfall may have been two-thirds of modern values at the time of the highest $\delta^{18}O$ values during Heinrich Stadial 1 (HS1) (16.1 ka) and one fifth again higher than modern values during the Bølling (14.3 ka). Within HS1, consistent with observations from other localities, Chinese cave records exhibit a twofold structure. Within the phases, we observe a truly remarkable relationship between the North Atlantic ice rafted debris record and the Hulu-Shima Cave record, where events ranging from multi-centennial to sub-decadal timescale can be related across Eurasia. The origin of this two-phased structure may relate to different sources and extent of ice-rafted debris in the North Atlantic as well as the extent of sea ice and the Atlantic Meridional Overturning Circulation.

* Corresponding author. School of Geography, Nanjing Normal University, Nanjing, 210023, China.
E-mail addresses: lucy2012_2015@163.com (Y. Liang), 09371@njnu.edu.cn (K. Zhao), edwar001@umn.edu (R.L. Edwards), yjwang@njnu.edu.cn (Y. Wang), 09396@njnu.edu.cn (Q. Shao), 1286246202@qq.com (Z. Zhang), 294546354@qq.com (B. Zhao), wangpowerful@163.com (Q. Wang), cheng021@xjtu.edu.cn (H. Cheng), xinggongkong@njnu.edu.cn (X. Kong).

https://doi.org/10.1016/j.quascirev.2020.106699
0277-3791/

1. Introduction

The last deglaciation (21–11 ka) was punctuated by many climate perturbations (Clark et al., 2012; Ng et al., 2018). Changes in the ice sheets and sea level (Denton et al., 2010; Lambeck et al., 2014), ocean circulation (McManus et al., 2004; Ng et al., 2018), the atmospheric-oceanic carbon cycle (Marcott et al., 2014; Bauska et al., 2016) and low-latitude hydroclimate (Wang et al., 2001; Weijers et al., 2007; Deplazes et al., 2013) are closely associated with millennial-scale events (e.g. Heinrich Stadial 1 (HS1) and Bølling-Allerød (BA)). HS1, one of the most prominent Heinrich stadials of the last ice age, features massive freshwater and iceberg discharge from the Northern Hemisphere ice sheets into the North Atlantic (Heinrich, 1988). Following HS1, the BA period is characterized by warm temperatures in the Northern Hemisphere (Marcott et al., 2014; WAIS Divide Project Members, 2015).

Whereas there have been considerable efforts on providing perspective on the orbital- and millennial-scale climate changes during the last deglacial period (Denton et al., 2010), higher resolution paleoclimate records extend investigations to the centennial-scale and can potentially provide a more precise understanding of processes during the deglaciation sequence (Marcott et al., 2014; Chen et al., 2015; Bauska et al., 2016). For example, three abrupt centennial-scale increases in atmospheric CO_2 (each of 10–15 ppmv) superimposed on the millennial-scale changes in the last deglaciation, and have been closely linked to CH_4 changes and Northern Hemisphere climate (Marcott et al., 2014). Two of these increases at around 14.8 ka and 11.7 ka were synchronous with the rapid intensification of the Asian monsoon and the abrupt recovery of the Atlantic Meridional Overturning Circulation (AMOC) (Chen et al., 2015). Heinrich events are believed to be associated with strong perturbations on the AMOC and global climate; however, with high-resolution records emerging, HS1 is found not to be one monotonous event and exhibit a two-phase structure (Bard et al., 2000; Broecker et al., 2009; Broecker and Putman., 2012; Huang et al., 2019), along with many other high frequency features (Brendryen et al., 2020). Chinese cave records have also documented a generally weak Asian Monsoon during HS1 (e.g. Wang et al., 2001), but some of the detailed characteristics and forcing mechanisms within this event are still not well understood. With our new record and the previously published Hulu record (Wang et al., 2001; Wu et al., 2009), we now have an opportunity to assess ideas with regard to submillennial-scale changes during the last deglaciation.

Studies about the interpretation of $\delta^{18}O$ in Asian caves have often stated that this is a controversial topic (e.g. Chiang et al., 2020). A clear reading of the literature shows that this is not now and has not historically been the case. Indeed, the literature shows that the essence of the interpretations put forth in the original papers on the subject (Wang et al., 2001; Yuan et al., 2004; Johnson and Ingram, 2004; Cheng et al., 2009) have been verified by subsequent empirical and theoretical studies (Liu et al., 2014; Orland et al., 2015; Cheng et al., 2012, 2016). This is not to say that there were not significant unknowns at the time of the early publications. A number of those unknowns have since been elucidated and others still remain. The literature, thus shows that the original publications, laid a solid foundation upon which subsequent publications built, with more work yet to come, in this ongoing, vibrant area of research. Here we use our new data along with published data to test some of the ideas regarding the interpretation of oxygen isotopes in Chinese caves. We then present our conclusions and assessment of the current state of this field.

Here we report a new $^{230}Th/U$-dated, high-resolution stalagmite $\delta^{18}O$ record spanning much of the early portion of the last deglaciation, from Shima Cave, Hunan Province, central China. This record covers about 4900 years, with an average oxygen isotope resolution of better than 7 years. The stalagmite grew continuously for 1900 years at the end of the last glacial maximum (LGM, 19.7–17.8 ka), then after a 1500-year hiatus, for another 3000 years, covering the last half of HS1, on into the BA (16.3–13.3 ka). We analyze this record in the context of other Asian cave records and other correlative records from around the world. Within this context, we examine the suite of records with the notion that HS1 is characterized by two stages as well as high-frequency features. In addition, we use our record and the now large number of published cave records across Asia to test ideas about the interpretation of the $\delta^{18}O$ of Chinese cave deposits. Since these records span a large geographic range, we can now use them to test models that hindcast shifts in $\delta^{18}O$ as a function of location.

2. Materials and methods

Stalagmite sample SM7 was collected from Shima Cave (Fig. 1, 29°35′N, 109°31′E), in Hunan Province of central China, ~930 km southwest of Hulu Cave (32°30′N, 119°10′E). The cave is at an elevation of ~650 m and is developed in Permian limestone, with a narrow entrance facing to the southwest. The cave site is strongly influenced by the East Asian Monsoon climate. Modern observational data from the nearest Enshi station (~80 km north of Shima Cave) shows that the mean annual temperature in this region is ~17 °C and the mean annual rainfall is ~1430 mm. Nearly 57% of precipitation falls from May to August (MJJA, the summer monsoon season (Ding and Chan, 2005)) with July being the wettest month. The variations in monthly simulated precipitation $\delta^{18}O$ values (Yoshimura et al., 2008) at Enshi have a seasonal amplitude larger than 7‰ over the year (Fig. 1), with the most negative monthly $\delta^{18}O$ value occurring in July and August and the most positive values during March and April. Moisture sources from the distant Indian Ocean, the Pacific Ocean and the Bay of Bengal prevail in the active East Asian Summer Monsoon (EASM) season (MJJA), together contributing two thirds of the precipitation near the cave site, with 31% of the water vapor derived from adjacent seas (Fig. S1).

A hiatus can be observed as a thin brownish layer occurring at a depth of 464 mm, which is also the boundary between an abrupt shift from yellowish-opaque calcite layers below the hiatus to pure and transparent calcite above the hiatus (Fig. 2). There is no sign of post-depositional corrosion or dissolution at the hiatus or anywhere else in the stalagmite. For stable isotope analyses, a total of 706 subsamples were measured using a Finnigan-MAT 253 mass spectrometer coupled with a Kiel Carbonate Device at the School of Geography, Nanjing Normal University, China. All results were reported in parts per mil (‰) relative to the Vienna Pee Dee Belemnite (VPDB). Replicate analyses of an international standard (NBS19) indicated long-term reproducibility, with precisions better than 0.06‰ for $\delta^{18}O$ and 0.05‰ for $\delta^{13}C$ at the 1σ level.

Twenty-four powdered subsamples for $^{230}Th/U$ dating were obtained by drilling along the stalagmite growth axis with a carbide dental drill. Part of the dating work was performed at the School of Geography, Nanjing Normal University and used procedures for U/Th chemical separation in Shao et al. (2017). The U/Th isotopic solutions were analyzed on a Neptune multi-collector inductively coupled plasma mass spectrometer (MC-ICP-MS) and the $^{230}Th/U$ ages were obtained using an interactive program as described in Shao et al. (2019). Those with marks were processed at the Department of Earth Science, University of Minnesota, following details in Edwards et al. (1987). Separate uranium and thorium extracts were measured using MC-ICP-MS, following the methods described in Shen et al. (2012) and Cheng et al. (2013). All of the speleothem ages are in stratigraphic order with 2σ analytical errors

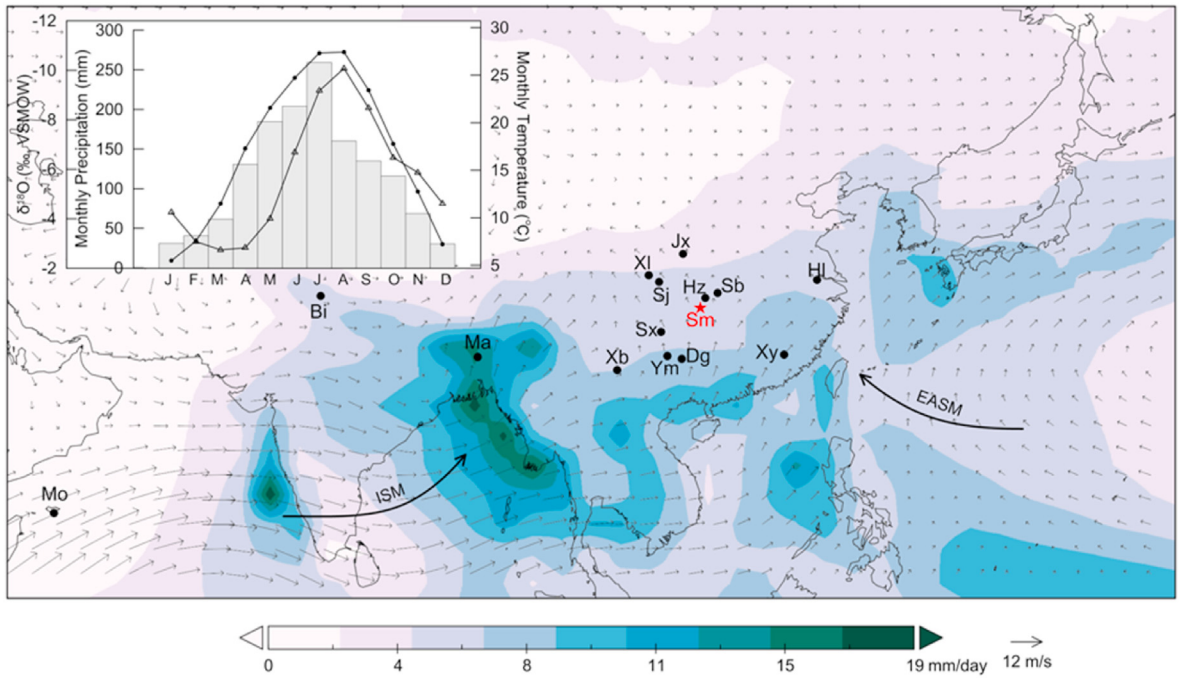

Fig. 1. Regional climatology and cave sites. NCEP/NCAR May to August (MJJA) daily precipitation (mm/day) and 850 hPa wind vectors (m/s) averaged from 1983 to 2012. Inset shows mean monthly rainfall and temperature (point) at Enshi station (30°16′N, 109°28′E) (https://gis.ncdc.noaa.gov/maps/ncei/cdo/monthly), and monthly simulated precipitation $\delta^{18}O$ (triangle) (Yoshimura et al., 2008). Arrows indicate the directions of the Indian Summer Monsoon (ISM) and the East Asian Summer Monsoon (EASM). Cave sites are: Sm-Shima Cave (this study, indicated by red star), Mo-Moomi Cave (Shakun et al., 2007), Bi-Bittoo Cave (Kathayat et al., 2016), Ma-Mawmluh Cave (Dutt et al., 2015), Xb-Xiaobailong Cave (Cai et al., 2015), Ym-Yamen Cave (Yang et al., 2010), Dg- Dongge Cave (Yuan et al., 2004), Sx-Sanxing Cave (Jiang et al., 2014), Xy-Xianyun Cave (Cui et al., 2017), Sm-Shima Cave (this study), Hz-Haozhu Cave (Zhang et al., 2018), Sb-Sanbao Cave (Wang et al., 2008), Sj-Songjia Cave (Zhou et al., 2008), Xl-Xianglong Cave (Li et al., 2019), Jx-Jiuxian Cave (Cai et al., 2010), Hl-Hulu Cave (Wang et al., 2001; Wu et al., 2009). (For interpretation of the references to colour in this figure legend, the reader is referred to the Web version of this article.)

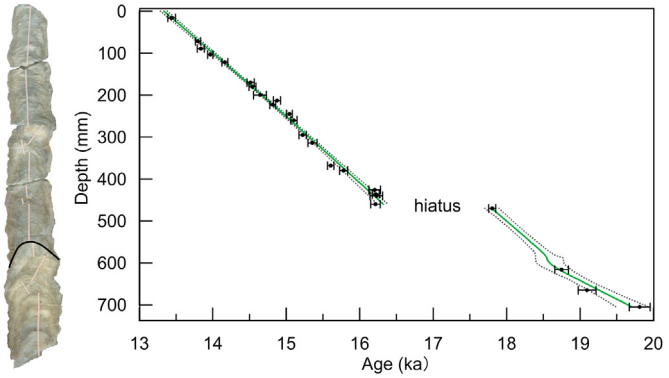

Fig. 2. The polished profile of SM7 (left panel) and the age model produced using MOD-AGE (right panel). Black dots and error bars indicate $^{230}Th/U$ ages and dating errors. Green lines and dashed lines represent the age median and 2σ results of MOD-AGE (Hercman and Pawlak, 2012). Black curve (at the depth of 464 mm) on the sample photo denotes hiatus. (For interpretation of the references to colour in this figure legend, the reader is referred to the Web version of this article.)

of roughly 0.3–0.7% (Table 1).

3. Results

3.1. Chronology

The U and Th isotopic compositions are presented in Table 1. Measured ^{238}U concentrations are low, ranging from 131.4 to 281.3 ppb. However, most of the samples have ^{232}Th concentrations less than 1000 ppt and relatively high $^{230}Th/^{232}Th$ activity ratios so that corrections for initial ^{230}Th are small. The length of time represented by the hiatus was determined to be ~1.5 ka, based upon extrapolation to 464 mm of the bounding ages drilled at 460 mm and 470 mm. Three dates at the lower part of the sample have significantly higher ^{232}Th content than the other samples and therefore have slightly higher uncertainties (over 90 years) associated with uncertainty in the correction for initial ^{230}Th. The age model for stalagmite SM7 was derived using MOD-AGE, which yielded the model age errors (Fig. 2) using Monte Carlo calculation (Hercman and Pawlak, 2012).

3.2. The $\delta^{18}O$ sequence

The $\delta^{18}O$ record covers the last deglaciation interval from 19.8 to 13.3 ka, yielding an average temporal resolution of less than 7 years (Fig. 3g). During the period from 19.8 to 17.7 ka (the end of the LGM), $\delta^{18}O$ values fluctuate about a mean value of −7.6‰. A prominent feature during the LGM cold interval are short-term perturbations (with cycles of ~400–500 years) in the monsoon system, indicating that the LGM does not reflect to be a monotonous event. This interval is followed by the 1.5-ka growth hiatus (the first part of HS1). At 16.3 ka, resumption of calcite precipitation is followed by a dramatic $\delta^{18}O$ increase from −6.3‰ to −4.7‰ centered at 16.1 ka and taking place over less than 40 years. About half of this shift takes place between two oxygen isotope drill holes, which based on growth rate, are different in age by 7 years. Thus, the rapidity of much of this shift is consistent with the observations of Treble et al. (2007), who concluded that much of the correlative shift at Hulu Cave took place in less than 2 years. These high $\delta^{18}O$ values, the highest values in the whole record, are maintained for 50 years before a gradual shift toward more negative values between 16.1 and 14.8 ka (the second part of HS1). This interval of gradual lowering of $\delta^{18}O$ ends with an abrupt, large-amplitude

Table 1
^{230}Th/U dating results for stalagmite SM7 from Shima Cave.

Sample	^{238}U		^{232}Th		^{230}Th/^{232}Th		δ^{234}U[a]		^{230}Th/^{238}U		^{230}Th Age (ka)		^{230}Th Age (ka)		$\delta^{234}U_{initial}$[b]	
Number	(ppb)		(ppt)		(atomic x10^{-6})		(measured)		(activity)		(uncorrected)		(corrected)		(corrected)	
SM7-16	131.4	±0.1	537.7	±10.0	987.3	±18.6	1073.3	±2.6	0.24489	±0.0007	13.49	±0.04	**13.44**	**±0.05**	1114.8	±2.7
SM7-72*	191.7	±0.2	165.2	±12.0	4889.9	±356.5	1117.2	±1.7	0.25564	±0.0005	13.88	±0.04	**13.89**	**±0.03**	1161.8	±1.8
SM7-89*	206.8	±0.2	578.8	±11.7	1512.7	±30.9	1117.3	±1.7	0.25677	±0.0006	13.94	±0.04	**13.91**	**±0.05**	1162.0	±1.7
SM7-103.5*	206.1	±0.2	332.8	±6.8	2659.7	±54.5	1131.4	±1.9	0.26049	±0.0005	14.06	±0.03	**14.04**	**±0.04**	1177.1	±2.0
SM7-121.5*	223.4	±0.2	557.1	±11.3	1726.2	±35.0	1106.2	±1.5	0.26104	±0.0005	14.27	±0.03	**14.24**	**±0.04**	1151.6	±1.6
SM7-170	222.2	±0.2	964.7	±13.6	1039.1	±14.9	1152.9	±2.4	0.27346	±0.0007	14.57	±0.04	**14.52**	**±0.05**	1201.1	±2.5
SM7-180*	259.8	±0.3	966.0	±19.4	1226.6	±24.7	1175.0	±2.1	0.27661	±0.0005	14.66	±0.03	**14.61**	**±0.05**	1224.4	±2.2
SM7-200	240.7	±0.3	572.1	±11.9	10314	±221	1154.4	±1.9	0.2754	±0.0015	14.74	±0.08	**14.64**	**±0.09**	1203	±2
SM7-213*	211.2	±0.2	702.9	±14.2	1375.3	±27.9	1138.0	±2.0	0.27761	±0.0006	14.99	±0.04	**14.94**	**±0.05**	1187.1	±2.0
SM7-223*	253.2	±0.2	635.5	±12.8	1828.1	±37.0	1152.4	±1.4	0.2783	±0.0005	14.92	±0.03	**14.89**	**±0.04**	1201.8	±1.5
SM7-245*	218.4	±0.2	477.3	±9.7	2111.4	±42.8	1134.4	±1.8	0.27984	±0.0005	15.14	±0.03	**15.11**	**±0.04**	1183.8	±1.9
SM7-260	210.1	±0.2	523.1	±12.6	1871.3	±45.3	1145.1	±2.4	0.28239	±0.0006	15.14	±0.04	**15.11**	**±0.04**	1195.0	±2.6
SM7-295*	241.8	±0.2	856.2	±17.2	1308.9	±26.4	1117.9	±2.0	0.28108	±0.0005	15.34	±0.04	**15.29**	**±0.05**	1167.2	±2.1
SM7-314*	246.0	±0.2	1235.2	±24.8	931.9	±18.8	1118.7	±2.0	0.28382	±0.0006	15.49	±0.04	**15.43**	**±0.06**	1168.5	±2.1
SM7-368*	202.6	±0.2	491.7	±9.9	1906.0	±38.7	1067.2	±1.7	0.28049	±0.0006	15.71	±0.04	**15.68**	**±0.04**	1115.4	±1.8
SM7-380	239.7	±0.1	633.8	±11.5	1801.5	±33.1	1105.6	±1.5	0.28878	±0.0008	15.82	±0.05	**15.78**	**±0.05**	1155.9	±1.6
SM7-426*	237.3	±0.3	1791.0	±36	675.5	±13.6	1190.3	±2.1	0.30914	±0.0006	16.37	±0.04	**16.27**	**±0.08**	1246.2	±2.2
SM7-436*	242.6	±0.2	682.4	±13.7	1797.5	±36.3	1178.2	±2.0	0.30661	±0.0006	16.33	±0.04	**16.29**	**±0.05**	1233.7	±2.1
SM7-440	274.5	±0.3	1267.2	±25.7	5755	±119	1117.5	±1.9	0.2985	±0.0012	16.36	±0.07	**16.23**	**±0.09**	1170	±2
SM7-460	226.8	±0.1	671.4	±10.1	1712	±26	1182.1	±1.2	0.3071	±0.0011	16.25	±0.06	**16.22**	**±0.06**	1237	±1
SM7-470	234.9	±0.2	599.6	±13.4	2202.5	±49.4	1220.4	±2.5	0.34085	±0.0007	17.84	±0.05	**17.81**	**±0.05**	1283.3	±2.6
SM7-616	281.3	±0.2	3128.1	±13.8	481.2	±2.3	1004.2	±2.2	0.32433	±0.0007	18.91	±0.05	**18.75**	**±0.09**	1058.7	±2.3
SM7-665	209.8	±0.2	3494.0	±13.6	348.4	±1.5	1128.7	±2.3	0.35165	±0.0007	19.32	±0.05	**19.09**	**±0.12**	1191.1	±2.5
SM7-705	235.9	±0.1	3926.6	±13.2	356.2	±1.8	1103.7	±1.3	0.35941	±0.0014	20.04	±0.09	**19.81**	**±0.14**	1167.1	±1.5

Corrected ^{230}Th ages assume the initial ^{230}Th/^{232}Th atomic ratio of $(4.4 \pm 2.2) \times 10^{-6}$. Those are the values for a material at secular equilibrium, with the bulk earth ^{232}Th/^{238}U value of 3.8. Errors are 2σ analytical errors. All ages are corrected to 'present' which is defined as the year 1950 AD.

[a] $\delta^{234}U = ([^{234}U/^{238}U]_{activity} - 1)x1000$.

[b] $\delta^{234}U_{initial}$ was calculated based on ^{230}Th age (T), i.e. $\delta^{234}U_{initial} = \delta^{234}U_{measured} \times e^{\lambda 234 \times T}$. U decay constants: $\lambda_{238} = 1.55125 \times 10^{-10}$ yr^{-1} (Jaffey et al., 1971) and $\lambda_{234} = 2.82206 \times 10^{-6}$ yr^{-1} (Cheng et al., 2013). Th decay constant: $\lambda_{230} = 9.1705 \times 10^{-6}$ yr^{-1} (Cheng et al., 2013).

* Ages are measured in University of Minnesota.

(~2‰) depletion centered at 14.65 ka (the shift into the BA). Most of this shift takes place within 100 years, consistent with the duration for the correlative shift observed at Hulu Cave (Cheng et al., 2016), Yamen Cave (Yang et al., 2010), and in Greenland ice (North Greenland Ice Core Project Members, 2004). $\delta^{18}O$ maintains those negative values for the remainder of the record, with the exception of a ~1‰ $\delta^{18}O$ enrichment at around 14.1 ka. Several centennial-scale fluctuations are also evident throughout the record. The general character of our record is broadly similar to many other records from across Asia (Fig. 3), although most other records have somewhat lower resolution than ours.

Isotopic equilibrium is a prerequisite for the climatic interpretation of calcite $\delta^{18}O$. The relatively low Pearson correlation between $\delta^{18}O$ and $\delta^{13}C$ ($r = 0.1$, $p < 0.01$, $n = 706$) in stalagmite SM7 is consistent with insignificant kinetic effects (Hendy, 1971). Our $\delta^{18}O$ record also shows good replication with other stalagmite records from the Asian monsoon domain in terms of general trends (Fig. 3): moderate $\delta^{18}O$ values during LGM, positive values during HS1 and very negative $\delta^{18}O$ values during the BA. Under isotopic equilibrium conditions (Dorale and Liu, 2009), the $\delta^{18}O$ signals of SM7 are mostly likely of climatic origin, indicating changes in the EASM.

4. Discussion

4.1. Controlling factors of Chinese stalagmite $\delta^{18}O$

The publication of the original Hulu Cave record (Wang et al., 2001) stimulated a long, fruitful, and ongoing debate on the interpretation of $\delta^{18}O$ values recorded in South and East Asian caves. With our new record and the now many records from across Asia, we have an opportunity to assess these ideas with regard to millennial-scale changes. Two mechanisms were proposed in the early studies, the Wang-Cheng Mechanism (Wang et al., 2001; Cheng et al., 2009) and the Yuan Mechanism (Yuan et al., 2004). Both have been expanded, connected to theory, and both have been shown to explain some of the variability in $\delta^{18}O$ observed in the cave records.

Wang et al. (2001) and Cheng et al. (2009) proposed that changing proportions of low $\delta^{18}O$ monsoon rainfall in annual totals could explain the observed cave $\delta^{18}O$ variability. Subsequent studies tested the Wang-Cheng mechanism (Dayem et al., 2010; Orland et al., 2015) and placed it on a theoretical basis (Orland et al., 2015; Chiang et al., 2015, 2020). These studies linked this mechanism to the position of the sub-tropical jet relative to the Tibetan Plateau. These authors noted (see Molnar et al., 2010) that the jet is south of the plateau during the winter, dry season in China, impinges on the southern edge of the plateau in spring when rainfall is moderate, and hits the plateau head on or even passes north of the plateau during the high rainfall summer monsoon season. Spring rainfall is unusually high in $\delta^{18}O$ and summer monsoon rainfall distinctly low. Thus, if in the past the jet spent a higher proportion of the year further to the south, southeastern China would likely have higher mean annual $\delta^{18}O$ and lower mean annual rainfall. Chiang et al. (2015, 2020) placed this idea on a theoretical basis providing a conceptual framework for the Wang-Cheng mechanism. Orland et al. (2015) measured $\delta^{18}O$ at seasonal resolution in a stalagmite collected from a cave in northeast China. Their data indicated that the Wang-Cheng mechanism could account for 25% of the shift in mean annual $\delta^{18}O$. Thus, we have one geographic point at the northern fringe of the monsoon showing the Wang-Cheng mechanism at work.

The Yuan Mechanism (Yuan et al., 2004), proposed in parallel with the Wang-Cheng mechanism, attributes cave variability to changing fractions of rainout resulting integrated between the

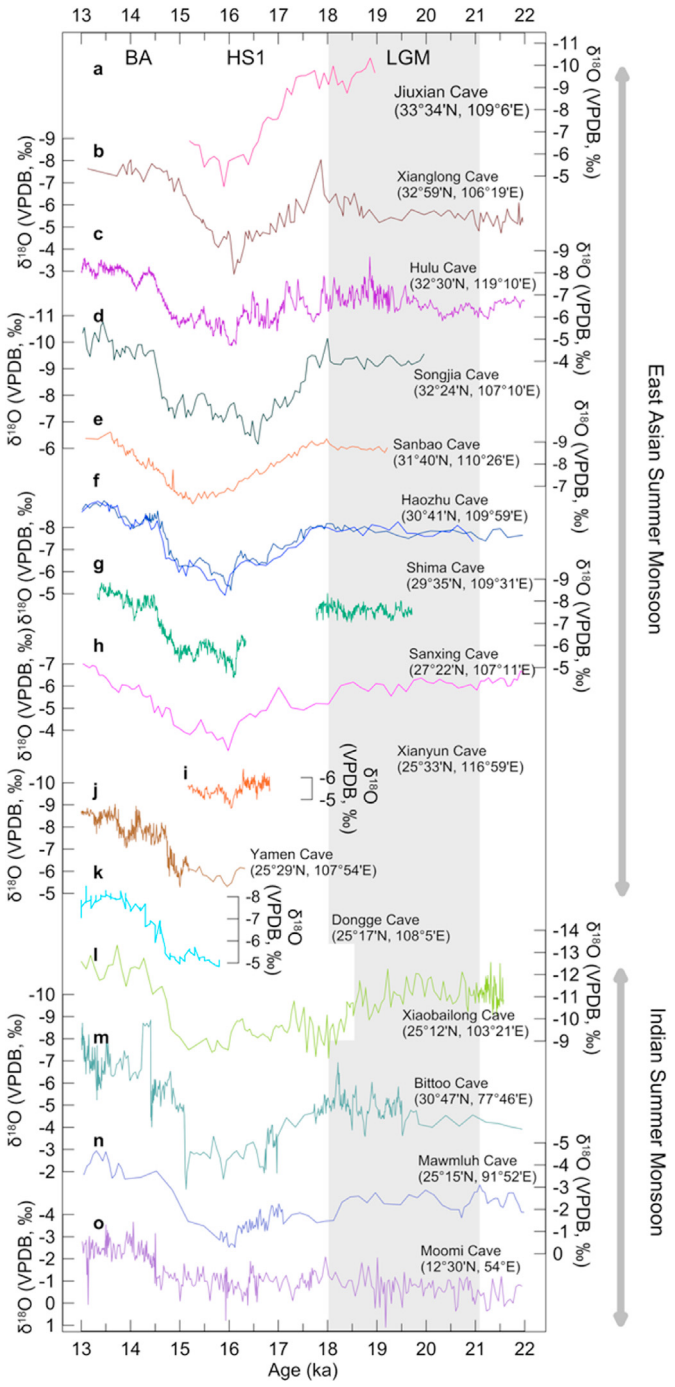

Fig. 3. Comparison between cave records from the Asian monsoon domain. Records are from: (a) Jiuxian Cave (Cai et al., 2010), (b) Xianglong Cave (Li et al., 2019), (c) Hulu Cave (Wang et al., 2001; Wu et al., 2009), (d) Songjia Cave (Zhou et al., 2008), (e) Sanbao Cave (Wang et al., 2008), (f) Haozhu Cave (Zhang et al., 2018), (g) Shima Cave (this study), (h) Sanxing Cave (Jiang et al., 2014), (i) Xianyun Cave (Cui et al., 2017), (j) Yamen Cave (Yang et al., 2010), (k) Dongge Cave (Yuan et al., 2004), (l) Xiaobailong Cave (Cai et al., 2015), (m) Bittoo Cave (Kathayat et al., 2016), (n) Mawmluh Cave (Dutt et al., 2015), (o) Moomi Cave (Shakun et al., 2007). The grey bar indicates time slice of LGM chosen for calculations.

tropical sources of water vapor (over the Pacific and Indian Oceans) and the cave sites. Using a standard Rayleigh fractionation model, Yuan et al. calculated the changing fraction of rainout required to explain the data. Combining this model with estimates of tropical ocean temperature and absolute humidity, they calculated the changes in integrated rainfall, which could explain the cave data. Hu et al. (2008) showed that some of the rainfall shift takes place in China. These initial studies were followed by a number of theoretical and empirical studies. Notably, a number of isotope-enabled modeling studies (LeGrande and Schmidt, 2006; Lewis et al., 2010; Pausata et al., 2011; Liu et al., 2014) examined the problem at both millennial and orbital timescales. These studies supported the idea that the Yuan mechanism was at least partially responsible for $\delta^{18}O$ variability observed in the cave records, although most modeling did not account for the full range of the observed variability. They also provided some theoretical framework for the process, either linked to orbital changes or to cold anomalies in the North Atlantic (e.g. hosing experiments simulating Heinrich events).

Of note is the Pausata et al. (2011) modeling study, as it makes specific predictions that we can test. The Pausata et al. model links a cold anomaly in the North Atlantic to increase in rainfall $\delta^{18}O$ in China via advection of cold air from the North Atlantic to the Indian Ocean. The cold anomaly reduces the Indian Ocean sea surface temperature, and lowers the fraction of rainout between the Indian Ocean moisture sources and cave sites, thereby raising $\delta^{18}O$ of rainfall in China. Most of the shift in model $\delta^{18}O$ results from changes in the Indian Ocean moisture sources. The location of much of the changes in model rainout is the upstream of eastern China; thus, suggesting that the Chinese cave variability largely records climate change west of eastern China. The Pausata et al. model uses LGM boundary conditions and predicts a pattern of $\delta^{18}O$ across southern Asia and China (Fig. 4).

Using our new data and those from caves across Asia (Fig. 3), we can now test some of these ideas. We first discuss the characteristics of the full set of records. The timing of the mid-HS1 monsoon weakening at 16.1 ka in our SM7 record agrees well with other stalagmite records from central China within dating errors. This monsoon weakening may correlate with a further southward migration of the Intertropical Convergence Zone (ITCZ) (Broecker and Putman., 2012). We observe nominal differences among these records. For caves north of 28°N (Fig. 3a–g), the $\delta^{18}O$ increases are large-amplitude (>1.5‰) and abrupt, occurring within decades (e.g. Hulu and Shima as mentioned before). However, for caves at lower latitudes (south of 28°N), the $\delta^{18}O$ can have smaller amplitudes (~1‰) (Fig. 3h–j). This could possibly be explained by the migration of the mid-latitude westerly jet which is closely related with the development of summer monsoon and controls the rain belt position in East Asia (Li et al., 2004; Sampe and Xie, 2010; Molnar et al., 2010). Under modern settings, prior to May, the westerly jet is located to the south of the Tibetan Plateau and situated at 25°N to 28°N (Li et al., 2004), inducing dry conditions at regions north of the wind belt axis but wet conditions in southern areas (Sampe and Xie, 2010). Rainfall discrepancies during pre-monsoon season are clearly seen at Shima/Hulu/Xianyun sites (Fig. 1 and Fig. S2). The pre-monsoon rainfall is also evident over the Indochina Peninsula (Kiguchi et al., 2016). Due to the impediment of the jet stream, only a small fraction of moisture-abundant maritime moisture can be transported into inland China (e.g. Shima and Hulu caves) but a large fraction can still reach the lower-latitude regions (e.g. Xianyun Cave) (Fig. S1). Afterwards, consistent with the jump of the westerly jet to the north of the Tibetan Plateau in May is the onset of the EASM, which gives way to the northward moisture-abundant ITCZ (Gadgil, 2018), leading to rainy conditions in southern China and an increasing contribution from remote oceans as far west as the Indian Ocean to cave sites. Major atmospheric circulation transitions related with the EASM development causes the consistent "valley-peak" pattern in precipitation $\delta^{18}O$ and rainfall increase at three sites (Fig. 1 and Fig. S2). Because the close linkage of the westerly jet path and the EASM at present can be used as an analogy in the past (Nagashima et al., 2011; Orland

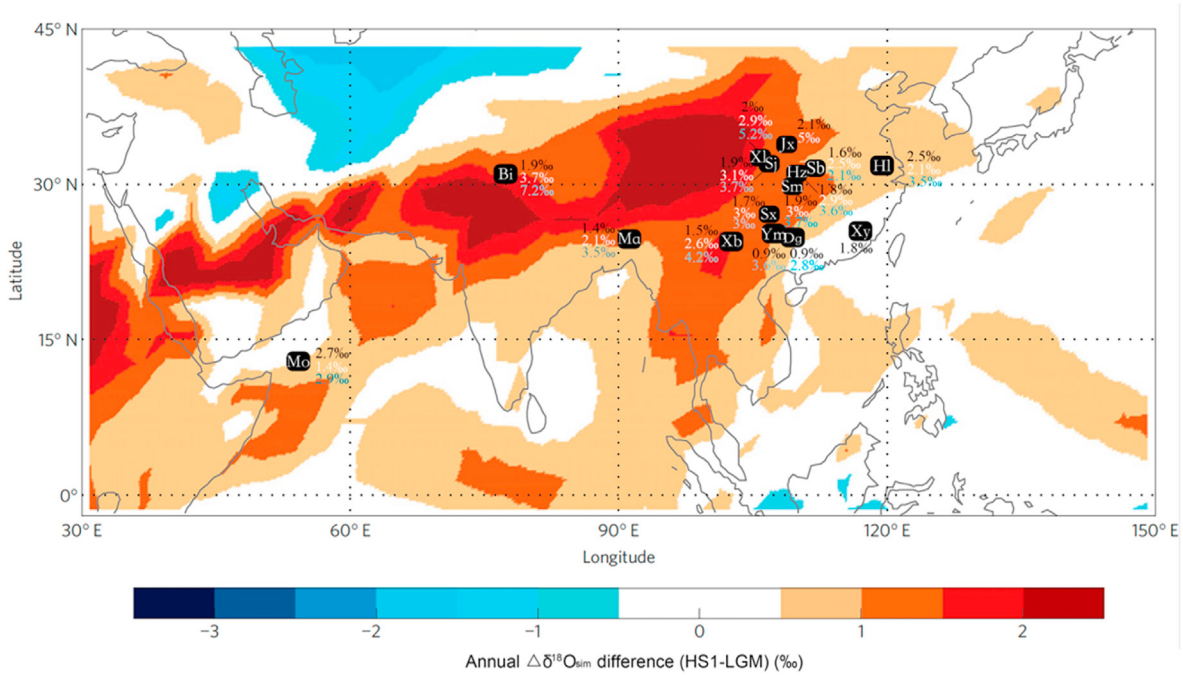

Fig. 4. Stalagmite $\delta^{18}O$ differences between the maximum value during HS1 and (1) the lowest value in HS1 (black, $\triangle\delta^{18}O_{HS1max-HS1min}$), (2) the average of the late LGM values (white, $\triangle\delta^{18}O_{HS1max-LGMave}$), and (3) the most negative value of the Bølling (B) warm period (blue, $\triangle\delta^{18}O_{HS1max-Bmin}$), plotted against the $\triangle\delta^{18}O_{sim}$ map modified from Pausata et al. (2011). Black rectangles indicate caves with the same labels as in Fig. 1. (For interpretation of the references to colour in this figure legend, the reader is referred to the Web version of this article.)

et al., 2015; Liang et al., 2019), we imply that at a pre-monsoon-like state (the 16.1-ka shift), less $\delta^{18}O$-depleted precipitation arrives at higher-latitude caves while lower-latitude caves could still be supplied with large amount of humid maritime moisture. A mixture of pre-monsoon rainfall and monsoonal rainfall could cause small-amplitude calcite $\delta^{18}O$ changes in these lower-latitude caves, thus leading to the regional differences in the 16.1-ka shift. This line of evidence addresses the importance of the westerly jet and the related Wang-Cheng mechanism on the $\delta^{18}O$.

We now compare the characteristics of the 15 cave records in Fig. 3 to the Pausata et al. predictions in Fig. 4. We calculated the shift in $\delta^{18}O$ values between the maximum value during HS1 (typically around 16 ka) and (1) the lowest value in HS1 ($\triangle\delta^{18}O_{HS1max-HS1min}$), (2) the average of the late LGM values ($\triangle\delta^{18}O_{HS1max-LGMave}$), and (3) the most negative value of the Bølling (B) warm period ($\triangle\delta^{18}O_{HS1max-Bmin}$) (Fig. 4) and compared those shifts with the mid-point of the contour interval for the modeled $\delta^{18}O$ differences (Fig. 5). We calculated the average LGM value by averaging the portion of the record between 21 and 18 ka, except for Xiaobailong Cave for which we averaged the plateau between 21 and 18.5 ka. We made an exception for Xiaobailong as the shift into HS1 takes place early relative to the other records, likely because ages have significant uncertainty in this time range (Cai et al., 2015). We reduced the difference for $HS1_{max}-B_{min}$ and $HS1_{max}-LGM_{ave}$ by −0.177‰/°C (Tremaine et al., 2011), assuming HS1 was 4 °C cooler than the B and 1 °C cooler than the LGM. We did not apply a temperature correction to $HS1_{max}-HS1_{min}$. In Fig. 5, we plotted the observation model discrepancy versus the percentage of moisture received from the Indian Ocean sources over the total percentage of moisture from the Pacific and the Indian Ocean sources for today's summer (MJJA).

A quick perusal of Figs. 4 and 5 shows that generally the model underestimates the observations. Of note is the fact that the vertical scale in Fig. 5 (−1‰ to +4‰ difference) is equal on the order of the full range of the whole Chinese record, so the deviations of points from a 0‰ difference is significant for many points. This is also the case for other isotope-enabled models (e.g. LeGrande and Schmidt, 2006; Lewis et al., 2010; Liu et al., 2014). Considering Fig. 5, the model comes closest to predicting the observations for $HS1_{max}-HS1_{min}$. This supports the idea that the model is most suited to simulating the specific instance of a hosing event rather than the full range of changes associated with a stadial-interstadial transition, e.g. the shift into the B.

Second, regardless of which of the three types of observations we consider, some of the biggest discrepancies are for cave sites which today receive a higher proportion of moisture from the Pacific sources. The discrepancy is nowhere more obvious than for Xianyun Cave (Cui et al., 2017) in Fujian Province, near the southeasternmost coast of China. The model predicts no change in $\delta^{18}O$ at this site, yet the Xianyun record shows the large and distinct HS1 high $\delta^{18}O$ anomaly common throughout China (Figs. 3 and 4). Of note is the fact that the Xianyun Cave site receives 88% of its summer season moisture from the Pacific (Fig. S1). Similar model underestimates are evident for our cave site and for Hulu Cave, both of which also have significant Pacific moisture sources. Indeed, in the EASM domain, $\triangle\delta^{18}O_{HS1max-LGMave}$ values are larger than $\triangle\delta^{18}O_{sim}$ by > 1‰ with no exceptions. Even within HS1, $\triangle\delta^{18}O_{HS1max-HS1min}$ values are larger than $\triangle\delta^{18}O_{sim}$ at most Chinese caves (Fig. 5a). These observations suggest that the Pausata et al. model may simulate changes in the Indian Monsoon, but does not appreciably capture changes that likely occurred in the East Asian Monsoon and the Pacific sourced moisture and rainfall. This finding is consistent with those of Li et al. (2019) and may be part of the explanation for why the Pausata et al. model predicts minimal rainfall change over China even though independent observations (Goldsmith et al., 2017; Beck et al., 2018) as well as some modeling studies (Zhang and Delworth, 2006; Liu et al., 2014) suggest otherwise.

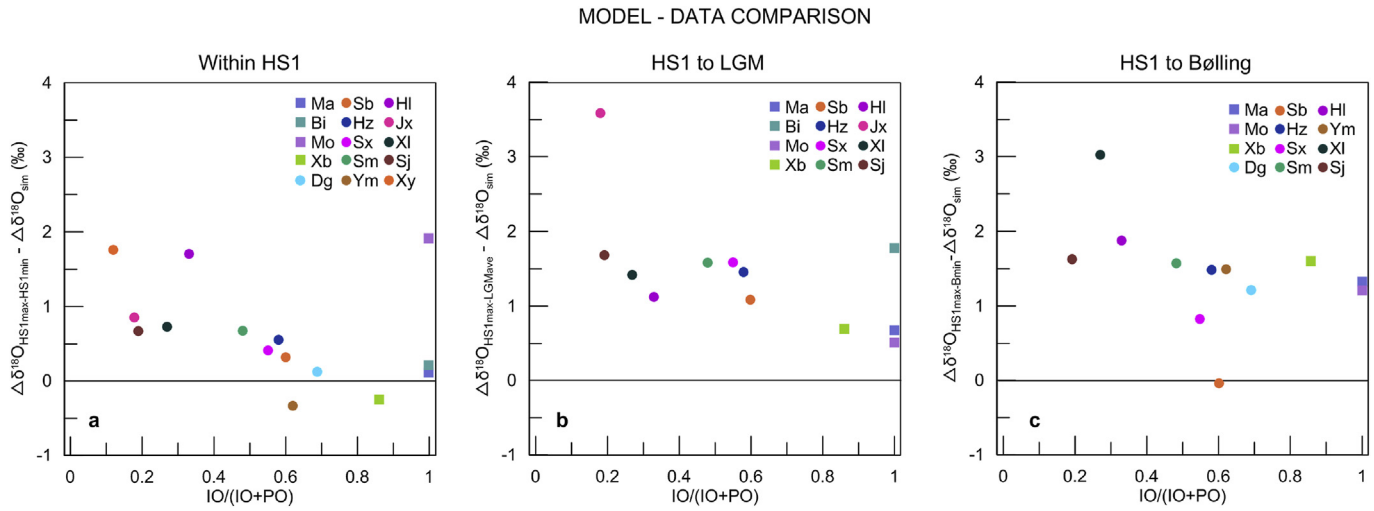

Fig. 5. Differences between the mid-point of the contour interval for the modeled $\delta^{18}O$ differences ($\triangle\delta^{18}O_{sim}$) and the observed cave $\delta^{18}O$ differences of (a) $\triangle\delta^{18}O_{Hmax-Hmin}$, (b) $\triangle\delta^{18}O_{Hmax-LGMave}$, and (c) $\triangle\delta^{18}O_{Hmax-Bmin}$. The X axis is the percentage of the Indian Ocean moisture component (IO) over the total percentage of moisture from the Pacific and the Indian Ocean sources (IO + PO), according to backward trajectory results for MJJA, 1983 to 2012. The difference between $\triangle\delta^{18}O_{Hmax-Bmin}$ and $\triangle\delta^{18}O_{sim}$ for Bittoo Cave is 4.7‰.

Combining our analysis with previous studies, we assess the current status of the interpretation of $\delta^{18}O$ in Chinese cave records as follows. Both the Wang-Cheng and Yuan mechanisms affect $\delta^{18}O$ in these records. We know that for one locality, the former is responsible for about 25% of the mean annual shift observed in the record (Orland et al., 2015). The Yuan mechanism has also affected $\delta^{18}O$ in Chinese Cave records and based upon the Orland et al. study, may be the dominant mechanism. The Yuan mechanism involves changes in rainfall integrated from both the Pacific and Indian Ocean sources. We do not know exactly how the changes in rainfall are partitioned along the moisture pathways. This should be a focus of future studies. For example, Zhang et al. (2018) aimed to tease out changes in the partitioning of rainfall changes within China, but their results were not robust, with, for example, different proxies within the same stalagmite implying changes in rainfall at different times. Nevertheless, it is clear that rainfall has changed at sites within China, including evidence from independent records that encompass HS1 (Goldsmith et al., 2017; Beck et al., 2018; Yu et al., 2020), observations that appear to be at odds with the results of Pausata et al. (2011).

In order to get a rough idea of the kinds of precipitation changes that might accompany the observed changes in $\delta^{18}O$, we calculated the changes of rainfall relative to the modern rainfall at our cave site for the B and $HS1_{max}$, subject to a number of simplifying assumptions. Those are: relative humidity in source regions constant with time (Sha et al., 2020); temperature during the B, 1 °C higher than present, temperature at $HS1_{max}$, 3 °C lower than present; change in fraction of moisture rained out constant from source to sink; Wang-Cheng mechanism responsible for 25% of the $\delta^{18}O$ difference from modern, Yuan mechanism responsible for 75% of the difference; and seawater $\delta^{18}O$ for $H1_{max}$ 0.80‰ higher, and for the B 0.60‰ higher. We calculated the rainfall shift due to the Wang-Cheng mechanism by adding or subtracting the number of average July days and adding or subtracting a third that number each of average April, May, and June days to achieve the target shift in $\delta^{18}O$. We then calculated mean annual rainfall based upon the altered number of average days for those 4 months. Three factors, then contributed to the percentage shift in rainfall relative to modern, the shift based upon the Wang-Cheng calculation, the shift based upon the change in fraction rained out in the standard Rayleigh calculation, and the shift in absolute humidity based upon the assumption of constant relative humidity and the assumed temperature difference in the source regions. Relative to modern, we calculate the percentage rainfall during the B to be 118% and for $HS1_{max}$ 66%. Given necessary assumptions these are rough numbers, but provide some estimate of the order of precipitation shifts.

4.2. Two phases of Heinrich Stadial 1

Investigations of ice rafted debris (IRD) deposition during Heinrich Stadial 1 suggest a structure that involves two large pulses (Bard et al., 2000; Gil et al., 2015; Hodell et al., 2017). In response to this long-lasting and two-stage Heinrich event, numerous studies not only show the far field effects of this event but also exhibit a two-phase structure. For example, Lake Estancia of New Mexico experienced Big Dry and Big Wet episodes over the course of HS1 (Broecker et al., 2009; Broecker and Putman., 2012). Records from the Congo Basin, Northwest Australia and Brazil indicated extremely dry conditions during early HS1 but wet conditions during late HS1 in the southern tropical regions (Weijers et al., 2007; Dupont et al., 2010; Denniston et al., 2017; Stríkis et al., 2018). In contrast, palaeoceanographic records from the northeastern Arabian Sea and the southern South China Sea, and hydrological reconstruction in the Dahu wetland, southern China suggest higher rainfall during early HS1 and lower rainfall during late HS1 (Deplazes et al., 2013; Huang et al., 2019; Yu et al., 2020). The interhemispheric anti-phased dry/wet conditions during HS1 seen in the global monsoon are considered to be linked with the displacement of the ITCZ (Denniston et al., 2017; Gadgil, 2018; Huang et al., 2019), and such two phases of the low-latitude hydroclimate are even apparent in the D-excess and ^{17}O-excess records in Greenland (Landais et al., 2018).

We use the IRD results from the following two sites as a means of comparing IRD records to our monsoon record below: one off the coast of Norway (65°45′N, 4°10′E; Brendryen et al., 2020 and the references therein) and one off of the Iberian Peninsula (37°46′N, 10°11′E; Bard et al., 2000). Both sites show an elevated flux of IRD as well as elevated values for other measures of ice rafting, covering the full HS1 interval, from 17.8 to 14.8 ka (Fig. 6). The similarity of these records suggests broadly in-phase behavior with ice-rafting from North America (the Iberian site) and Europe (the Norwegian

site). There are two major pulses starting at the beginning of each of the two HS1 phases that we suggest (HS1a (17.8–16.1 ka) and HS1b (16.1–14.8 ka)). Focusing on the more northerly site, within HS1a, there are two additional significant, but smaller peaks, separated by a background of somewhat elevated IRD. Within HS1b, there is one additional smaller IRD peak with, again, elevated background between the peaks and extending after the second peak to around 14.8 ka, the end of HS1. Frequent and intensive IRD releases from the European ice sheet during HS1 are also evident in other studies (e.g. Dokken and Jansen, 1999; Toucanne et al., 2015). The more southerly site has lower resolution, but largely the same structure as the northerly site. It also has key pieces of information, notably that the large peak at the beginning of the first phase includes dominantly detrital carbonate, sourced from Hudson Straits and the large peak at the beginning of the second phase is much higher in magnetic susceptibility than the peak at the beginning of the first phase. The one at the beginning of the second phase, is dominated by quartz grains, some of which are hematite-stained. Although the source of the latter is not absolutely clear, a strong candidate are sandstones from the Labrador region (Gil et al., 2015).

A remarkable relationship is found between the North Atlantic IRD records and the Chinese cave records. Considering our record, the first hint of a two-phased structure in the monsoon is the fact that our stalagmite has a hiatus covering HS1a. Unfortunately, there are multiple reasons for hiatuses in speleothems, including but not limited to the idea that this represents a dry interval. Fortunately, the Hulu Cave record covers HS1a in high resolution (Wang et al., 2001; Wu et al., 2009). Thus, we can compare the combined Hulu-Shima cave record with the North Atlantic IRD records (Bard et al., 2000; Brendryen et al., 2020 and references therein). The most remarkable aspect of this comparison is the fact that the peaks in the higher resolution IRD record (Fig. 6d) correspond to troughs in the Hulu-Shima record (Fig. 6e), the three in HS1a and the two in HS1b. This relationship is consistent with the general relationship between the North Atlantic and the monsoon, e.g. Greenland interstadials correspond to inferred wet conditions and Greenland stadials correspond to inferred dry conditions in monsoonal portions of China (Wang et al., 2001). However, here we observe this relationship at extremely high resolution, multi-centennial to even sub-decadal timescales.

A comparison between the Hulu-Shima record and the Greenland ice core $\delta^{18}O$ record illustrates two points (Fig. 6). First, the $\delta^{18}O$ difference of the average between two phases in the monsoon record exceeds 0.5‰, more than 1/3 the amplitude of the standard Dansgaard-Oeschger events as recorded in Hulu Cave (Wang et al., 2001), with HS1b higher in $\delta^{18}O$ (drier in inferred conditions) than HS1a. This parallels the shift in inferred temperature in Greenland from with lower average temperature during the second phase of HS1 (Fig. 6a). Second, Greenland has nowhere near the structure and fluctuations within HS1 as the monsoon (Landais et al., 2018). This confirms the known limited structure to Greenland ice core $\delta^{18}O$ within Heinrich stadials, even though there is clear evidence in the near field (e.g. the IRD records discussed here) as well as the far field (e.g. our cave records) for substantial climate change in the North Atlantic region as well as elsewhere during these intervals.

According to $^{231}Pa/^{230}Th$ records from the North Atlantic (Fig. 6b) (McManus et al., 2004; Gherardi et al., 2005; Böhm et al., 2015; Mulitza et al., 2017; Ng et al., 2018), the AMOC was nearly in the "off" mode across HS1 but relatively weaker during HS1b. A compilation of deep Atlantic sedimentary $^{231}Pa/^{230}Th$ records further suggest a two-phased AMOC reduction in HS1; the early slowdown and the subsequent maximum reduction (Ng et al., 2018). Because the AMOC is widely believed to modulate global climate (e.g. McManus et al., 2004; Ng et al., 2018), its twostep changes may explain why there are two phases of climatic change within HS1 worldwide, including the EASM; because the EASM is also likely linked to the AMOC through the migration of the ITCZ (Chiang and Friedman, 2012; Gadgil, 2018).

Taken together, there is strong evidence that cold conditions or processes expected to result from cold conditions in the North Atlantic result in inferred dry conditions in the monsoonal regions of China. This is consistent with observations from the earliest Chinese cave records (e.g. Wang et al., 2001) and broadly consistent with many modeling studies (e.g. Zhang and Delworth, 2006; Lewis et al., 2010; Pausata et al., 2011; Liu et al., 2014). However, in the context of HS1, this extends to its two phases, which we infer fundamentally to the shift from a sluggish AMOC to a yet more sluggish AMOC. It also extends to multi-centennial-scale features to sub-decadal features within each phase of HS1. In this regard, it is likely that the formation of sea ice (in association with the measures of the North Atlantic climate that we have discussed) plays an important role because the cooling and expansion of sea ice are strongly associated with ice-rafting events (Gil et al., 2015). Denton et al. (2005) pointed out that formation of the North Atlantic sea ice would result in cold European winters and likely contribute to suppressing the monsoon and the ITCZ. Pausata et al. (2011) showed that sea ice was important in generating a significant response in monsoon $\delta^{18}O$ in their model. In this regard, much of the rapid shift (<2 years, Treble et al., 2007; <7 years as documented here) into the first high $\delta^{18}O$ excursion HS1b (at 16.1 ka), may result from rapid expansion of sea ice, as this is one phenomenon that could change at that rapid pace (Gildor and Tziperman, 2000).

5. Conclusions

A new $^{230}Th/U$ dated, ~7-year-resolution stalagmite $\delta^{18}O$ record from Shima Cave, Hunan Province, provides us with new evidence into the interpretation of speleothem $\delta^{18}O$ and the millennial-to sub-decadal-scale monsoon variations during the early portion of the last deglaciation. Our sample SM7 grew in time periods from 19.7 to 13.3 ka, with a ~1500-year hiatus (from 17.8 to 16.3 ka). The record resembles other Chinese cave records and features the abrupt shift to the highest $\delta^{18}O$ values in the Chinese record at 16.1 ka and the abrupt shift into the Bølling at 14.65 ka.

Using new and existing Indian region and Chinese speleothem records, we compare simulated $\delta^{18}O$ changes in Pausata et al. (2011) with observed shifts in $\delta^{18}O$ in Asian caves. We find that the model generally underestimates the observations in these three cases: within HS1, between the LGM and HS1 and between the B and HS1. Some of the biggest discrepancies are for cave sites which receive a higher proportion of moisture from the Pacific Ocean, suggesting that the Pausata et al. model may not appreciably capture changes that likely occurred in the East Asian Monsoon domain. Along with other sets of observations and theoretical studies, we conclude the following regarding the interpretation of $\delta^{18}O$ in Chinese caves. $\delta^{18}O$ are affected by two mechanisms: changes in the fraction of monsoon rainfall in annual totals (the Wang-Cheng mechanism) and changes in the amount of integrated rainout between tropical sources and cave sites (the Yuan mechanism). Within this context, we make rough calculations for Shima site, which suggests that mean annual rainfall may have been two thirds of modern values at the time of the highest $\delta^{18}O$ values during HS1 and one fifth again higher than modern values during the Bølling warm period.

According to a detailed investigation into the high-resolution SM7 and H82 records, HS1 can be divided into two phases, the early weakening, fluctuating monsoon from 17.8 to 16.1 ka (HS1a) and a weaker EASM condition from 16.1 to 14.8 ka (HS1b). The step-

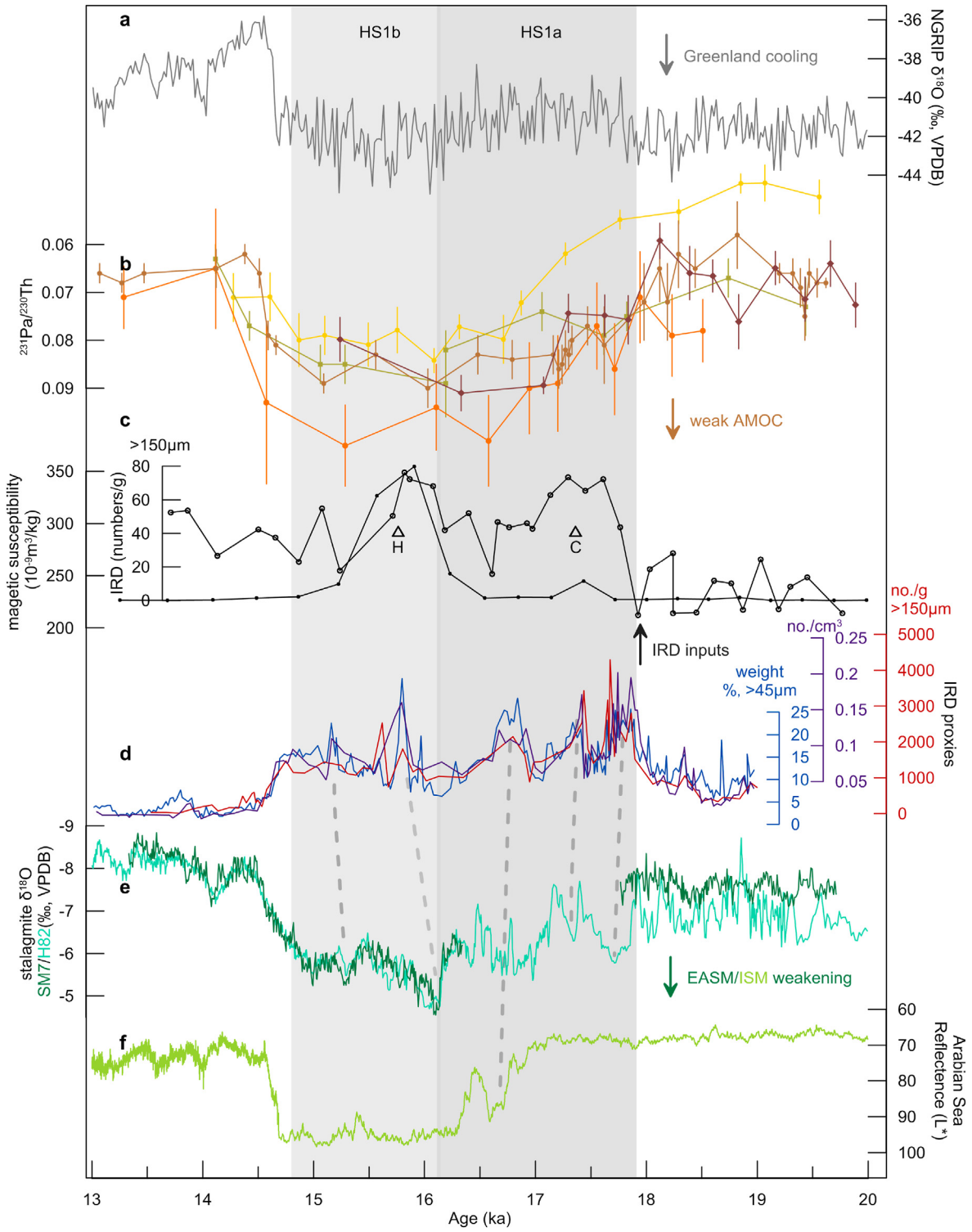

Fig. 6. Comparison of geological records over HS1. (a) $\delta^{18}O$ record of NGRIP ice core on the GICC05 chronology (North Greenland Ice Core Project Members, 2004; Svensson et al., 2008). (b) $^{231}Pa/^{230}Th$ records from the North Atlantic sedimentary cores (brown: McManus et al., 2004; yellow: Gherardi et al., 2005; orange: Mulitza et al., 2017; dark brown: Böhm et al., 2015; olive: Ng et al., 2018). (c) IRD counts (black dots) and magnetic susceptibility (hollow circles) records off the coast of Iberian Peninsula (Bard et al., 2000). Mineralogical markers are: C for detrital carbonates and H for hematite-coated grains. (d) Proxy records of IRD from the Norwegian Sea cores (Brendryen et al., 2020 and references therein). (e) $\delta^{18}O$ records of SM7 from Shima Cave and H82 from Hulu Cave (Wang et al., 2001; Wu et al., 2009). (f) Reflectance record of the Arabian Sea core (Deplazes et al., 2013). Grey and light grey bars indicate the early and late HS1, respectively. Dashed lines indicate corresponding IRD peaks and the weak EASM events within HS1. (For interpretation of the references to colour in this figure legend, the reader is referred to the Web version of this article.)

wise monsoon is likely related to the observed changes in the AMOC intensity during HS1. There are 5 significant inferred dry pulses in the monsoon, three in HS1a and two in HS1b. All correspond to IRD peaks in the record from off of Norway. We infer that the dry periods are the response of the monsoon to cold anomalies in the North Atlantic at the multi-centennial to sub-decadal scale. We also infer that sea ice formation plays a role, particularly in the onset of the large inferred dry period starting at 16.1 ka, which takes place in less than 2 years.

Author statement

Yijia Liang: Conceptualization, Formal analysis, Funding acquisition, Investigation, Writing - original draft. Kan Zhao: Writing-Reviewing and Editing, Project administration, Funding acquisition. R. Lawrence Edwards: Conceptualization, Funding acquisition, Writing- Reviewing and Editing. Yongjin Wang: Writing- Reviewing and Editing, Funding acquisition. Qingfeng Shao: Formal analysis, Investigation. Zhenqiu Zhang: Investigation, Resources. Bin Zhao: Investigation, Resources. Quan Wang: Formal analysis, Funding acquisition. Hai Cheng: Investigation. Xinggong Kong: Investigation, Funding acquisition.

Declaration of competing interest

The authors declare that they have no known competing financial interests or personal relationships that could have appeared to influence the work reported in this paper.

Acknowledgement

We thank Editor Dr. Miryam Bar-Matthews and two anonymous reviewers for their constructive comments. This work was supported by National Natural Science Foundation of China (Grants 42071105, 41931178, 41572151, 41571102, 41672164), the U.S. National Science Foundation (Grant 1702816), the Postgraduate Research & Practice Innovation Program of Jiangsu Province (Grant KYCX19_0789), the 111 Program of China (Grant D19002), the Science and Technology Research Program of Chongqing Municipal Education Commission (Grant KJQN201900536) and the Open Fund for the State Key Laboratory of Loess and Quaternary Geology (Grant SKLLQG 1922).

Appendix A. Supplementary data

Supplementary data to this article can be found online at https://doi.org/10.1016/j.quascirev.2020.106699.

References

Bard, E., Rostek, F., Turon, J.L., Gendreau, S., 2000. Hydrological impact of Heinrich events in the subtropical northeast Atlantic. Science 289, 1321–1324.
Bauska, T.K., Baggenstos, D., Brook, E.J., Mix, A.C., Marcott, S.A., Petrenko, V.V., Schaefer, H., Severinghaus, J.P., Lee, J.E., 2016. Carbon isotopes characterize rapid changes in atmospheric carbon dioxide during the last deglaciation. Proc. Natl. Acad. Sci. Unit. States Am. 113, 3465–3470.
Beck, J.W., Zhou, W., Li, C., Wu, Z., White, L., Xian, F., Kong, X., An, Z., 2018. A 550,000-year record of East Asian monsoon rainfall from ^{10}Be in loess. Science 360, 877–881.
Böhm, E., Lippold, J., Gutjahr, M., Frank, M., Blaser, P., Antz, B., Fohlmeister, J., Frank, N., Andersen, M.B., Deininger, M., 2015. Strong and deep Atlantic meridional overturning circulation during the last glacial cycle. Nature 517, 73–76.
Brendryen, J., Haflidason, H., Yokoyama, Y., Haaga, K.A., Hannisdal, B., 2020. Eurasian Ice Sheet collapse was a major source of Meltwater Pulse 1A 14,600 years ago. Nat. Geosci. 13, 363–368.
Broecker, W.S., McGee, D., Adams, K.D., Cheng, H., Edwards, R.L., Oviatt, C.G., Quade, J., 2009. A Great Basin-wide dry episode during the first half of the Mystery Interval? Quat. Sci. Rev. 28, 2557–2563.
Broecker, W.S., Putnam, A.E., 2012. How did the hydrologic cycle respond to the two-phase mystery interval? Quat. Sci. Rev. 57, 17–25.
Cai, Y., Tan, L., Cheng, H., An, Z., Edwards, R.L., Kelly, M.J., Kong, X., Wang, X., 2010. The variation of summer monsoon precipitation in central China since the last deglaciation. Earth Planet Sci. Lett. 291, 21–31.
Cai, Y., Fung, I.Y., Edwards, R.L., An, Z., Cheng, H., Lee, J.E., Tan, L., Shen, C.C., Wang, X., Day, J.A., Zhou, W., 2015. Variability of stalagmite-inferred Indian monsoon precipitation over the past 252,000 y. Proc. Natl. Acad. Sci. Unit. States Am. 112, 2954–2959.
Chen, T., Robinson, L.F., Burke, A., Southon, J., Spooner, P., Morris, P.J., Ng, H.C., 2015. Synchronous centennial abrupt events in the ocean and atmosphere during the last deglaciation. Science 349, 1537–1541.
Cheng, H., Edwards, R.L., Broecker, W.S., Denton, G.H., Kong, X., Wang, Y., Zhang, R., Wang, X., 2009. Ice age terminations. Science 326, 248–252.
Cheng, H., Sinha, A., Wang, X., Cruz, F.W., Edwards, R.L., 2012. The Global paleomonsoon as seen through speleothem records from Asia and the Americas. Clim. Dynam. 39, 1045–1062.
Cheng, H., Edwards, R.L., Shen, C., Polyak, V.J., Asmerom, Y., Woodhead, J., Hellstrom, J., Wang, Y., Kong, X., Spötl, C., 2013. Improvements in ^{230}Th dating, ^{230}Th and ^{234}U half-life values, and U-Th isotopic measurements by multi-collector inductively coupled plasma mass spectrometry. Earth Planet Sci. Lett. 371, 82–91.
Cheng, H., Edwards, R.L., Sinha, A., Spötl, C., Yi, L., Chen, S., Kelly, M., Kathayat, G., Wang, X., Li, X., Kong, X., Wang, Y., Ning, Y., Zhang, H., 2016. The Asian monsoon over the past 640,000 years and ice age terminations. Nature 534, 640–646.
Chiang, J.C.H., Friedman, A.R., 2012. Extratropical cooling, interhemispheric thermal gradients, and tropical climate change. Annu. Rev. Earth Planet Sci. 40, 383–412.
Chiang, J.C., Fung, I.Y., Wu, C.H., Cai, Y., Edman, J.P., Liu, Y., Day, J.A., Bhattacharya, T., Mondal, Y., Labrousse, C.A., 2015. Role of seasonal transitions and westerly jets in East Asian paleoclimate. Quat. Sci. Rev. 108, 111–129.
Chiang, J.C., Herman, M.J., Yoshimura, K., Fung, I.Y., 2020. Enriched East Asian oxygen isotope of precipitation indicates reduced summer seasonality in regional climate and westerlies. Proc. Natl. Acad. Sci. Unit. States Am. 117, 14745–14750.
Clark, P.U., Shakun, J.D., Baker, P.A., Bartlein, P.J., Brewer, S., Brook, E., Carlson, A.E., Cheng, H., Kaufman, D.S., Liu, Z., Marchitto, T.M., Mix, A.C., Morrill, C., Otto-Bliesner, B.L., Pahnke, K., Russell, J.M., Whitlock, C., Adkins, J.F., Blois, J.L., Clark, J., Colman, S.M., Curry, W.B., Flower, B.P., He, F., Johnson, T.C., Lynch-Stieglitz, J., Markgraf, V., McManus, J., Mitrovica, J.X., Moreno, P.I., Williams, J.W., 2012. Global climate evolution during the last deglaciation. Proc. Natl. Acad. Sci. Unit. States Am. 109, E1134–E1142.
Cui, M., Xiao, H., Sun, X., Hong, H., Jiang, X., Cai, B., 2017. Characteristics of the Heinrich 1 abrupt climate event inferred from a speleothem record from Xianyun Cave, Fujian Province. Sci. Bull. 62, 3078–3088.
Dayem, K.E., Molnar, P., Battisti, D.S., Roe, G.H., 2010. Lessons learned from oxygen isotopes in modern precipitation applied to interpretation of speleothem records of paleoclimate from eastern Asia. Earth Planet Sci. Lett. 295, 219–230.
Denniston, R.F., Asmerom, Y., Polyak, V.J., Wanamaker Jr., A.D., Ummenhofer, C.C., Humphreys, W.F., Cugley, J., Woods, D., Lucker, S., 2017. Decoupling of monsoon activity across the northern and southern Indo-Pacific during the Late Glacial. Quat. Sci. Rev. 176, 101–105.
Denton, G.H., Alley, R.B., Comer, G.C., Broecker, W.S., 2005. The role of seasonality in abrupt climate change. Quat. Sci. Rev. 24, 1159–1182.
Denton, G.H., Anderson, R.F., Toggweiler, J.R., Edwards, R.L., Schaefer, J.M., Putnam, A.E., 2010. The last glacial termination. Science 328, 1652–1656.
Deplazes, G., Lückge, A., Peterson, L.C., Timmermann, A., Hamann, Y., Hughen, K.A., Röhl, U., Laj, C., Cane, M.A., Sigman, D.M., Haug, G.H., 2013. Links between tropical rainfall and North Atlantic climate during the last glacial period. Nat. Geosci. 6, 213–217.
Ding, Y., Chan, J.C., 2005. The East Asian summer monsoon: an overview. Meteorol. Atmos. Phys. 89, 117–142.
Dokken, T.M., Jansen, E., 1999. Rapid changes in the mechanism of ocean convection during the last glacial period. Nature 401, 458–461.
Dorale, J.A., Liu, Z., 2009. Limitations of Hendy test criteria in judging the paleoclimatic suitability of speleothems and the need for replication. J. Cave Karst Stud. 71, 73–80.
Dupont, L.M., Schlütz, F., Ewah, C.T., Jennerjahn, T.C., Paul, A., Behling, H., 2010. Two-step vegetation response to enhanced precipitation in Northeast Brazil during Heinrich event 1. Global Change Biol. 16, 1647–1660.
Dutt, S., Gupta, A.K., Clemens, S.C., Cheng, H., Singh, R.K., Kathayat, G., Edwards, R.L., 2015. Abrupt changes in Indian summer monsoon strength during 33,800 to 5500 years B. P. Geophys. Res. Lett. 42, 5526–5532.
Edwards, R.L., Chen, J., Wasserburg, G., 1987. ^{238}U-^{234}U-^{230}Th-^{232}Th systematics and the precise measurement of time over the past 500,000 years. Earth Planet Sci. Lett. 81, 175–192.
Gadgil, S., 2018. The monsoon system: land-sea breeze or the ITCZ? J. Earth Syst. Sci. 127, 1. https://doi.org/10.1007/s12040-017-0916-x.
Gherardi, J.M., Labeyrie, L., McManus, J.F., Francois, R., Skinner, L.C., Cortijo, E., 2005. Evidence from the Northeastern Atlantic basin for variability in the rate of the meridional overturning circulation through the last deglaciation. Earth Planet Sci. Lett. 240, 710–723.
Gil, I.M., Keigwin, L.D., Abrantes, F., 2015. The deglaciation over Laurentian Fan: history of diatoms, IRD, ice and fresh water. Quat. Sci. Rev. 129, 57–67.
Gildor, H., Tziperman, E., 2000. Sea ice as the glacial cycles climate switch: role of seasonal and orbital forcing. Paleoceanography 15, 605–615.

Goldsmith, Y., Broecker, W.S., Xu, H., Polissar, P.J., Demenocal, P.B., Porat, N., Lan, J., Cheng, P., Zhou, W., An, Z., 2017. Northward extent of East Asian monsoon covaries with intensity on orbital and millennial timescales. Proc. Natl. Acad. Sci. Unit. States Am. 114, 1817–1821.
Heinrich, H., 1988. Origin and consequences of cyclic ice rafting in the Northeast Atlantic Ocean during the past 130,000 years. Quat. Res. 29, 142–152.
Hendy, C.H., 1971. The isotopic geochemistry of speleothems-I. The calculation of the effects of different modes of formation on the isotopic composition of speleothems and their applicability as palaeoclimatic indicators Geochim. Cosmochim. Acta 3, 801–824.
Hercman, H., Pawlak, J., 2012. MOD-AGE: an age-depth model construction algorithm. Quat. Geochronol. 12, 1–10.
Hodell, D.A., Nicholl, J.A., Bontognali, T.R., Danino, S., Dorador, J., Dowdeswell, J.A., Einsle, J., Kuhlmann, H., Martrat, B., Mleneck-Vautravers, M.J., Rodríguez-Tovar, F.J., 2017. Anatomy of Heinrich Layer 1 and its role in the last deglaciation. Paleoceanography 32, 284–303.
Hu, C., Henderson, G.M., Huang, J., Xie, S., Sun, Y., Johnson, K.R., 2008. Quantification of Holocene Asian monsoon rainfall from spatially separated cave records. Earth Planet Sci. Lett. 266, 221–232.
Huang, J., Wan, S., Li, A., Li, T., 2019. Two-phase structure of tropical hydroclimate during Heinrich Stadial 1 and its global implications. Quat. Sci. Rev. 222, 105900. https://doi.org/10.1016/j.quascirev.2019.105900.
Jaffey, A.H., Flynn, K.F., Glendenin, L.E., Bentley, W.C., Essling, A.M., 1971. Precision measurement of half-lives and specific activities of ^{235}U and ^{238}U. Phys. Rev. C 4, 1889–1906.
Jiang, X., He, Y., Shen, C., Lee, S.Y., Yang, B., Lin, K., Li, Z., 2014. Decoupling of the East Asian summer monsoon and Indian summer monsoon between 20 and 17 ka. Quat. Res. 82, 146–153.
Johnson, K.R., Ingram, B.L., 2004. Spatial and temporal variability in the stable isotope systematics of modern precipitation in China: implications for paleoclimate reconstructions. Earth Planet Sci. Lett. 220, 365–377.
Kathayat, G., Cheng, H., Sinha, A., Spötl, C., Edwards, R.L., Zhang, H., Li, X., Yi, L., Ning, Y., Cai, Y., Lui, W.L., 2016. Indian monsoon variability on millennial-orbital timescales. Sci. Rep. 6, 24374. https://doi.org/10.1038/srep24374.
Kiguchi, M., Matsumoto, J., Kanae, S., Oki, T., 2016. Pre-monsoon rain and its relationship with monsoon onset over the Indochina Peninsula. Front. Earth Sci. 4, 42. https://doi.org/10.3389/feart.2016.00042.
Lambeck, K., Rouby, H., Purcell, A., Sun, Y., Sambridge, M., 2014. Sea level and global ice volumes from the last glacial maximum to the holocene. Proc. Natl. Acad. Sci. Unit. States Am. 111, 15296–15303.
Landais, A., Capron, E., Masson-Delmotte, V., Toucanne, S., Rhodes, R., Popp, T., Vinther, B., Minster, B., Prié, F., 2018. Ice core evidence for decoupling between midlatitude atmospheric water cycle and Greenland temperature during the last deglaciation. Clim. Past 14, 1405–1415.
LeGrande, A.N., Schmidt, G.A., 2006. Global gridded data set of the oxygen isotopic composition in seawater. Geophys. Res. Lett. 33, L12604. https://doi.org/10.1029/2006GL026011.
Lewis, S.C., LeGrande, A.N., Kelley, M., Schmidt, G.A., 2010. Water vapour source impacts on oxygen isotope variability in tropical precipitation during Heinrich events. Clim. Past 6, 325–343.
Li, C., Wang, Z., Lin, S., Gao, H., 2004. The relationship between East Asian Summer Monsoon activity and northward jump of the upper westerly jet location. Chin. J. Atmos. Sci. 5, 641–658.
Li, D., Tan, L., Cai, Y., Jiang, X., Ma, L., Cheng, H., Edwards, R.L., Zhang, H., Gao, Y., An, Z., 2019. Is Chinese stalagmite δ^{18}O solely controlled by the Indian summer monsoon? Clim. Dynam. 53, 2969–2983.
Liang, Y., Wang, Y., Wang, Q., Wu, J., Shao, Q., Zhang, Z., Yang, S., Kong, X., Edwards, R.L., 2019. East Asian summer monsoon climates and cave hydrological cycles over Dansgaard-Oeschger events 14 to 11 revealed by a new stalagmite record from Hulu Cave. Quat. Res. 92, 725–737.
Liu, Z., Wen, X., Brady, E.C., Otto-Bliesner, B., Yu, G., Lu, H., Cheng, H., Wang, Y., Zheng, W., Ding, Y., Edwards, R.L., 2014. Chinese cave records and the East Asia summer monsoon. Quat. Sci. Rev. 83, 115–128.
Marcott, S.A., Bauska, T.K., Buizert, C., Steig, E.J., Rosen, J.L., Cuffey, K.M., Fudge, T.J., Severinghaus, J.P., Ahn, J., Kalk, M.L., McConnell, J.R., Sowers, T., Taylor, K.C., White, J.W.C., Brook, E.J., 2014. Centennial-scale changes in the global carbon cycle during the last deglaciation. Nature 514, 616–619.
McManus, J.F., Francois, R., Gherardl, J.M., Kelgwin, L., Drown-Leger, S., 2004. Collapse and rapid resumption of Atlantic meridional circulation linked to deglacial climate changes. Nature 428, 834–837.
Molnar, P., Boos, W.R., Battisti, D.S., 2010. Orographic controls on climate and paleoclimate of Asia: thermal and mechanical roles for the Tibetan Plateau. Annu. Rev. Earth Planet Sci. 38, 77–102.
Mulitza, S., Chiessi, C.M., Schefuß, E., Lippold, J., Wichmann, D., Antz, B., Mackensen, A., Paul, A., Prange, M., Rehfeld, K., Werner, M., 2017. Synchronous and proportional deglacial changes in Atlantic meridional overturning and northeast Brazilian precipitation. Paleoceanography 32, 622–633.
Nagashima, K., Tada, R., Tani, A., Sun, Y., Isozaki, Y., Toyoda, S., Hasegawa, H., 2011. Millennial-scale oscillations of the westerly jet path during the last glacial period. J. Asian Earth Sci. 40, 1214–1220.
Ng, H.C., Robinson, L.F., McManus, J.F., Mohamed, K.J., Jacobel, A.W., Ivanovic, R.F., Gregoire, L.J., Chen, T., 2018. Coherent deglacial changes in western Atlantic Ocean circulation. Nat. Commun. 9, 1–10.
North Greenland Ice Core Project Members, 2004. High-resolution record of Northern Hemisphere climate extending into the last interglacial period. Nature 431, 147–151.
Orland, I.J., Edwards, R.L., Cheng, H., Kozdon, R., Cross, M., Valley, J.W., 2015. Direct measurements of deglacial monsoon strength in a Chinese stalagmite. Geology 43, 555–558.
Pausata, F.S., Battisti, D.S., Nisancioglu, K.H., Bitz, C.M., 2011. Chinese stalagmite δ^{18}O controlled by changes in the Indian monsoon during a simulated Heinrich event. Nat. Geosci. 4, 474–480.
Sampe, T., Xie, S.P., 2010. Large-scale dynamics of the meiyu–baiu rainband: environmental forcing by the westerly jet. J. Clim. 23, 113–134.
Sha, L., Mahata, S., Duan, P., Luz, B., Zhang, P., Baker, J., Zong, B., Ning, Y., Ait Brahim, Y., Zhang, H., Edwards, R.L., Cheng, H., 2020. A novel application of triple oxygen isotope ratios of speleothems. Geochim. Cosmochim. Acta 270, 360–378.
Shakun, J.D., Burns, S.J., Fleitmann, D., Kramers, J., Matter, A., Al-Subary, A., 2007. A high-resolution, absolute-dated deglacial speleothem record of Indian Ocean climate from Socotra Island, Yemen. Earth Planet Sci. Lett. 259, 442–456.
Shao, Q., Pons-Branchu, E., Zhu, Q., Wang, W., Valladas, H., Fontugne, M., 2017. High precision U/Th dating of the rock paintings at Mt. Huashan, Guangxi, southern China. Quat. Res. 88, 1–13.
Shao, Q., Li, C., Huang, M., Liao, Z., Arps, J., Huang, C., Chou, Y., Kong, X., 2019. Interactive programs of MC-ICPMS data processing for ^{230}Th/U geochronology. Quat. Geochronol. 51, 43–52.
Shen, C., Wu, C., Cheng, H., Edwards, R.L., Hsieh, Y.T., Gallet, S., Chang, C., Li, T., Lam, D.D., Kano, A., Hori, M., Spötl, C., 2012. High-precision and high-resolution carbonate ^{230}Th dating by MC-ICP-MS with SEM protocols. Geochem. Cosmochim. Acta 99, 71–86.
Stríkis, N.M., Cruz, F.W., Barreto, E.A., Naughton, F., Vuille, M., Cheng, H., Voelker, A.H., Zhang, H., Karmann, I., Edwards, R.L., Auler, A.S., 2018. South American monsoon response to iceberg discharge in the North Atlantic. Proc. Natl. Acad. Sci. Unit. States Am. 115, 3788–3793.
Svensson, A., Andersen, K.K., Bigler, M., Clausen, H.B., Dahl-Jensen, D., Davies, S.M., Johnsen, S.J., Muscheler, R., Parrenin, F., Rasmussen, S.O., Röthlisberger, R., Seierstad, I., Steffensen, J.P., Vinther, B.M., 2008. A 60,000 year Greenland stratigraphic ice core chronology. Clim. Past 3, 47–57.
Toucanne, S., Soulet, G., Freslon, N., Jacinto, R.S., Dennielou, B., Zaragosi, S., Eynaud, F., Bourillet, J.F., Bayon, G., 2015. Millennial-scale fluctuations of the European Ice Sheet at the end of the last glacial, and their potential impact on global climate. Quat. Sci. Rev. 123, 113–133.
Treble, P.C., Schmitt, A.K., Edwards, R.L., McKeegan, K.D., Harrison, T.M., Grove, M., Cheng, H., Wang, Y.J., 2007. High resolution secondary ionisation mass spectrometry (SIMS) δ^{18}O analyses of Hulu Cave speleothem at the time of Heinrich Event 1. Chem. Geol. 238, 197–212.
Tremaine, D.M., Froelich, P.N., Wang, Y., 2011. Speleothem calcite farmed in situ: modern calibration of δ^{18}O and δ^{13}C paleoclimate proxies in a continuously-monitored natural cave system. Geochem. Cosmochim. Acta 75, 4929–4950.
WAIS Divide Project Members, 2015. Precise interpolar phasing of abrupt climate change during the last ice age. Nature 520, 661–665.
Wang, Y., Cheng, H., Edwards, R.L., An, Z., Wu, J., Shen, C., Dorale, J.A., 2001. A high-resolution absolute-dated late Pleistocene monsoon record from Hulu Cave, China. Science 294, 2345–2348.
Wang, Y., Cheng, H., Edwards, R.L., Kong, X., Shao, X., Chen, S., Wu, J., Jiang, X., Wang, X., An, Z., 2008. Millennial-and orbital-scale changes in the East Asian monsoon over the past 224,000 years. Nature 451, 1090–1093.
Weijers, J.W.H., Schefuß, E., Schouten, S., Damsté, J.S.S., 2007. Coupled thermal and hydrological evolution of tropical Africa over the last deglaciation. Science 315, 1701–1704.
Wu, J., Wang, Y., Cheng, H., Edwards, R.L., 2009. An exceptionally strengthened East Asian summer monsoon event between 19.9 and 17.1 ka BP recorded in a Hulu stalagmite. Sci. China Earth Sci. 52, 360–368.
Yang, Y., Yuan, D., Cheng, H., Zhang, M., Qin, J., Lin, Y., Zhu, X., Edwards, R.L., 2010. Precise dating of abrupt shifts in the Asian Monsoon during the last deglaciation based on stalagmite data from Yamen Cave, Guizhou Province, China. Sci. China Earth Sci. 53, 633–641.
Yoshimura, K., Kanamitsu, M., Noone, D., Oki, T., 2008. Historical isotope simulation using Reanalysis atmospheric data. J. Geophys. Res. Atm. 113, D19108. https://doi.org/10.1029/2008JD010074.
Yu, X., Chen, J., Zheng, Y., Zhong, W., Ouyang, Z., Zhou, W., 2020. Anti-phase variation of hydrology and in-phase carbon accumulations in two wetlands in southern and northern China since the last deglaciation. Front. Earth Sci. 8, 192. https://doi.org/10.3389/feart.2020.00192.
Yuan, D., Cheng, H., Edwards, R.L., Dykoski, C.A., Kelly, M.J., Zhang, M., Qing, J., Lin, Y., Wang, Y., Wu, J., Dorale, J.A., An, Z., Cai, Y., 2004. Timing, duration, and transitions of the last interglacial asian monsoon. Science 304, 575–578.
Zhang, H., Griffiths, M.L., Chiang, J.C., Kong, W., Wu, S., Atwood, A., Huang, J., Cheng, H., Ning, Y., Xie, S., 2018. East Asian hydroclimate modulated by the position of the westerlies during Termination I. Science 362, 580–583.
Zhang, R., Delworth, T.L., 2006. Impact of Atlantic multidecadal oscillations on India/Sahel rainfall and Atlantic hurricanes. Geophys. Res. Lett. 33, L17712. https://doi.org/10.1029/2006GL026267.
Zhou, H., Zhao, J., Feng, Y., Gagan, M.K., Zhou, G., Yan, J., 2008. Distinct climate change synchronous with Heinrich event one, recorded by stable oxygen and carbon isotopic compositions in stalagmites from China. Quat. Res. 69, 306–315.